IBRO Reports 7 (2019) 10–25

Contents lists available at ScienceDirect

IBRO Reports

journal homepage: www.elsevier.com/locate/ibror

Research Paper

# Mechanism of forelimb motor function restoration in rats with cervical spinal cord hemisection-neuroanatomical validation-

Hideaki Ohne[a,*], Masahito Takahashi[a], Kazuhiko Satomi[b], Atsushi Hasegawa[a], Takumi Takeuchi[a], Shunsuke Sato[a], Shoichi Ichimura[a]

[a] Department of Orthopaedic Surgery, Kyorin University School of Medicine, 6-20-2 Shinkawa Mitaka, Tokyo, 181-8611, Japan
[b] Orthopaedic Surgery, Kugayama Hospital, 2-14-20 Kitakarasuyama Setagaya, Tokyo, 157-0061, Japan

ARTICLE INFO

*Keywords:*
Neuro-tracing
Cervical spinal cord hemisection
Motor function restoration
Image J
Quantitative evaluation of immunostaining specimens
Nerve regeneration

ABSTRACT

*Purpose:* The purpose of this study is neuroanatomical validation of forelimb motor function restoration in rats with cervical spinal cord injury.

*Materials and methods:* We used eight cervical hemisected rats and eight normal rats. We cut in half the C3/4 cervical spinal cord of 18-weeks-old normal rats. We used 24-weeks-old rats that had reached a nearly steady state of forelimb motor function after the hemisection (Hemisection group). Normal 24-week-old rats were used as Control group. To evaluate the corticospinal tracts, neuro-tracing by biotynirated dextran-amine (BDA) was used. BDA was injected into the damaged side of the cerebral primary motor cortex. In order to quantitatively analyze the specimen, we recorded a site where nerve fibers appear in each specimen in the image analysis (1) and defined the increase rate of immunostaining area using ImageJ in the image analysis (2). Based on the evaluation in the image analysis (1) and the image analysis (2), the Hemisection group and the Control group were compared.

*Results:* In the image analysis (1), a region with robust appearance of aberrant nerve fibers was observed in the cephalad side of the Hemisection site in Hemisection group than Control group. In the spinal cord caudal to the hemisection, such region was generally more in Hemisection group, however, disappeared or reduced appearance was observed in some regions. In the image analysis (2), no statistical significant difference was noted in each level.

*Conclusion:* There is a high probability that these aberrant nerve fibers beyond the midline could be involved in forelimb motor function restoration in rats with cervical cord hemisection.

## Introduction

Motor paralysis from central nervous system injury is generally considered permanent, with axonal damage causing loss of neural network function (Martinez et al., 2009; Takahashi et al., 2009; Cajal, 1928). However, we have reported large-scale circuit remodeling in the corticospinal tract and recovery of forelimb motor function in a juvenile rat model of brain injury (Takahashi et al., 2009). In addition, we performed a longitudinal behavioral assessment in rats after cervical spinal cord hemisection, reporting that forelimb motor function had reached a steady state approximately four weeks after cervical hemisection and had recovered by 34% at the end of our assessment six weeks after hemisection (Hasegawa et al., 2016). Furthermore, we demonstrated that the forelimb motor function lost after spinal cord injury was restored by construction of compensatory pathway through electrophysical verification in hemisection rats (Takeuchi et al., 2017). However, neuroanatomical details of compensatory pathway remained unclear.

The purpose of this study was to neuroanatomical validation whether compensatory pathways exist in the corticospinal tract of rats which have recovered motor function following cerebral spinal cord hemisection.

## Materials and methods

This study was conducted with the approval of the Ethics Committee at Kyorin University.

* Corresponding author.
*E-mail address:* onehide0922@ybb.ne.jp (H. Ohne).

https://doi.org/10.1016/j.ibror.2019.05.002
Received 13 November 2018; Accepted 5 May 2019

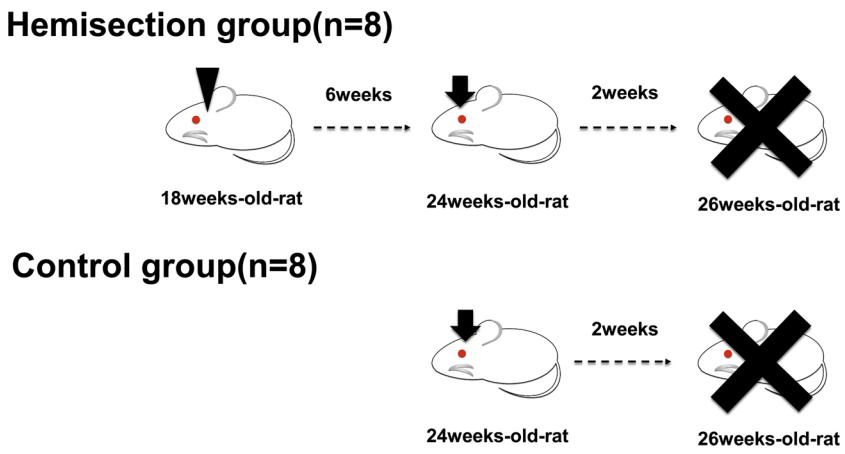


**Fig. 1.** Diagram of creation of Hemisection group and Control group. arrowhead: lesion (hemisection C3/4cervical spinal cord). arrow: BDA injection. cross mark: sacrifice.

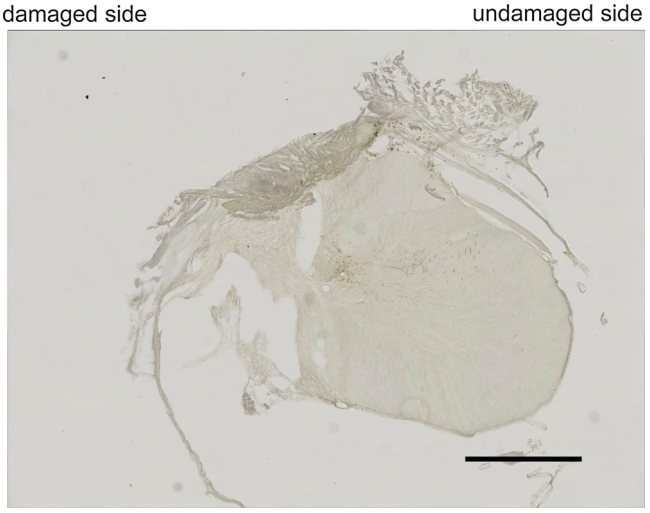


**Fig. 2.** Photomicrograph of Hemisection site (Scale bar = 1 mm).

*Animals*

A total of sixteen male 24-weeks-old Wistar rats, eight rats with cervical spinal cord hemisection (Hemisection group) and eight normal rats (Control group) were used. Since forelimb motor function in the hemisected rats reaches a steady state approximately four weeks after hemisection, the rats were used six weeks after hemisection (Fig. 1).

*Spinal cord injury and animal care*

For the cervical spinal hemisection, healthy 18-week-old rats (300–360 g) were fully anesthetized with an intraperitoneal injection of xylazine (0.1 mg/kg; Bayer Health Care, Monheim, Germany) and ketamine (3.6 mg/kg; Daiichi Sankyo, Tokyo, Japan) and a partial laminectomy was performed on C3 and C4 to expose the dura mater. An incision was made in the dura mater and arachnoid membrane to expose the dorsal aspect of the spinal cord, and a segmental hemisection approximately 2 mm wide was made in the left cervical spinal cord at this level (Fig. 2). After the hemisection, we performed intracranial stimulation using needle electrodes inserted 1.5 cm into the skin on

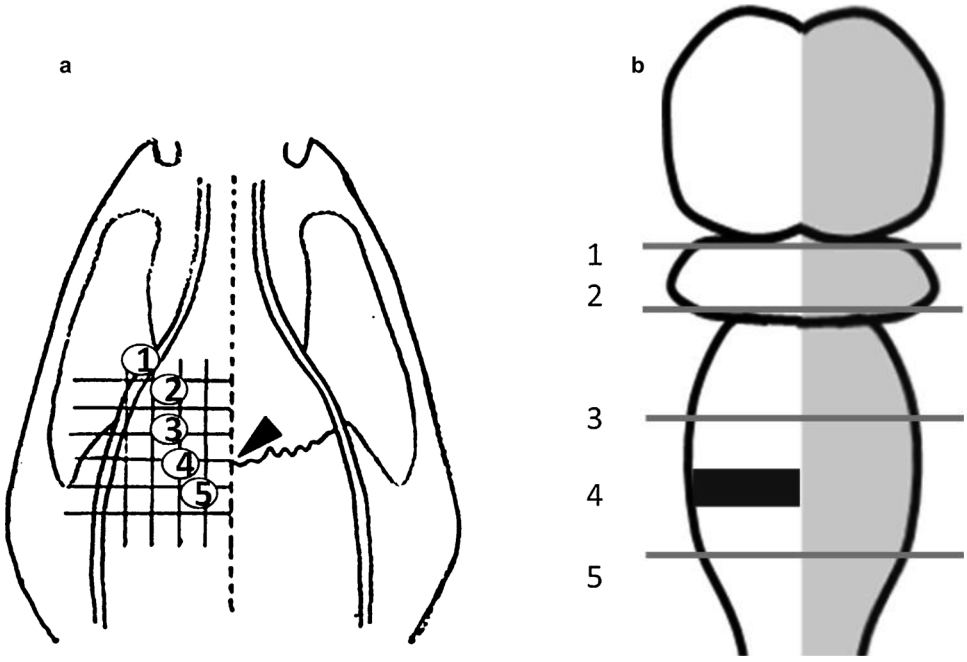


**Fig. 3.** (a) Diagram of injection site of the rat brain. We chose five injection sites in the primary motor cortex (M1) as a guide with Bregma as the zero point. Point (anterior, lateral, depth). Bregma (0 mm, 0 mm, 0 mm). (1) (3.72 mm,3.5 mm,3.0 mm). (2) (2.76 mm, 2.5 mm,2.0 mm). (3) (1.28 mm,2.5 mm, 2.0 mm). (4) (0.0 mm,2.0 mm,2.0 mm). (5) (-1.32 mm,1.5 mm,2.0 mm). Bregma (arrowhead). Injection site ((1), (2), (3), (4), (5)). (b) Diagram of specimens of rat brain and cervical spinal cord (hemisection rat). (1) Medulla cephalad to pyramidal decussation. (2) Medulla caudal to pyramidal decussation. (3) Cervical spinal cord cephalad to the hemisection. (4) Hemisection site. (5) Cervical spinal cord caudal to the hemisection.

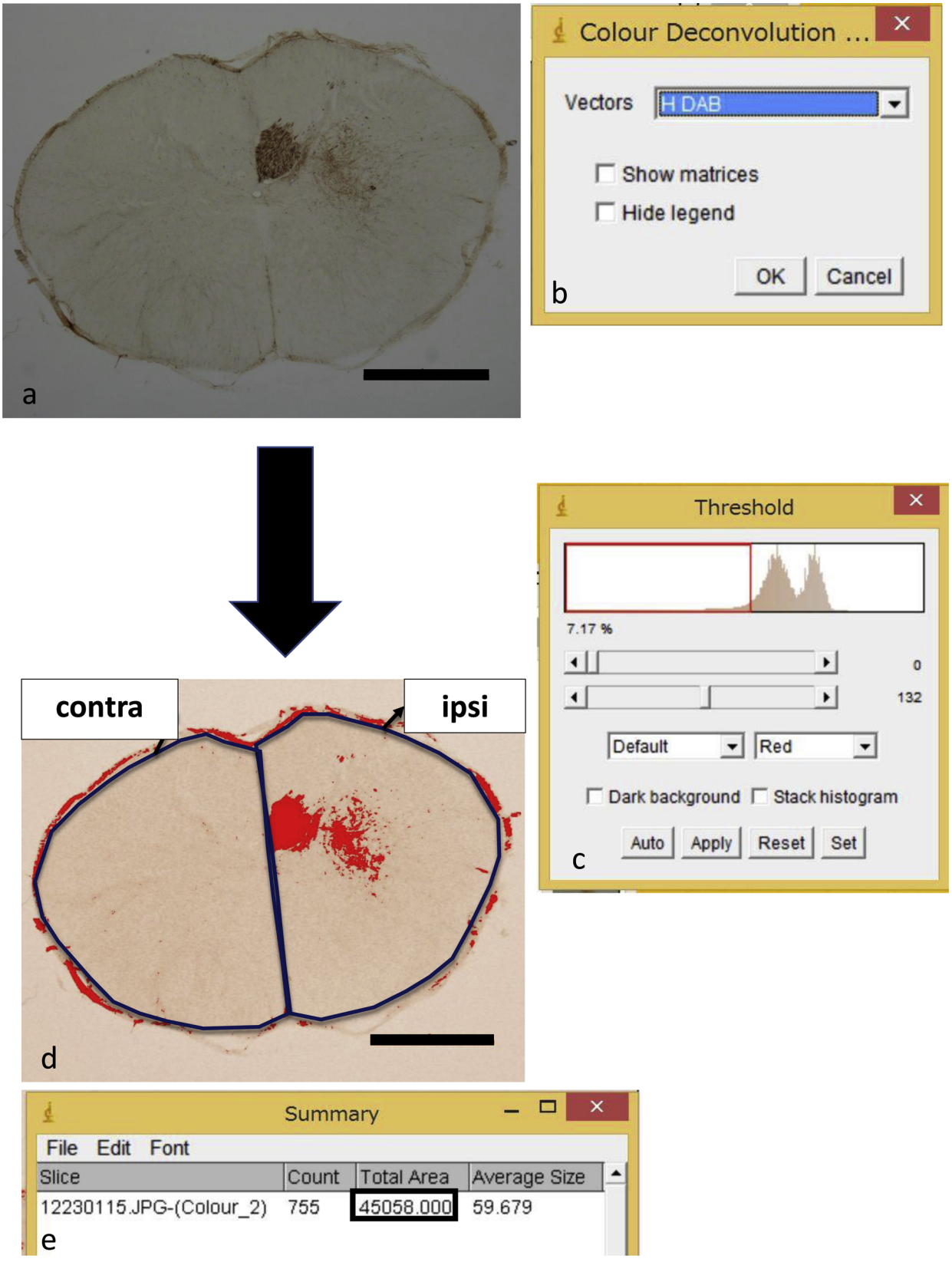


**Fig. 4.** Imaging data analysis and calculation of increase rate of the immunostaining area using ImageJ. a: Images were opened from ImageJ's File menu (Scale bar = 1 mm). b: To separate the hematoxylin and BDA immunostaining from the original sample image, RGB color separation was performed by selecting the H DAB vector in the Color Deconvolution plugin. c: After RGB color separation, the color thresholds were set with Image > Adjust > Threshold, so that only the DAB-immunostained fibers could be colored. d: Since the staining also labeled structures which were clearly not nerve fibers, such as the pia mater, we trimmed the images with the polygon selection tool to include only the areas where nerve fibers were stained(Scale bar = 1 mm). e: we used Analyse > Analyse Particles > Summarize to calculate the Total Area positive for immunostaining.

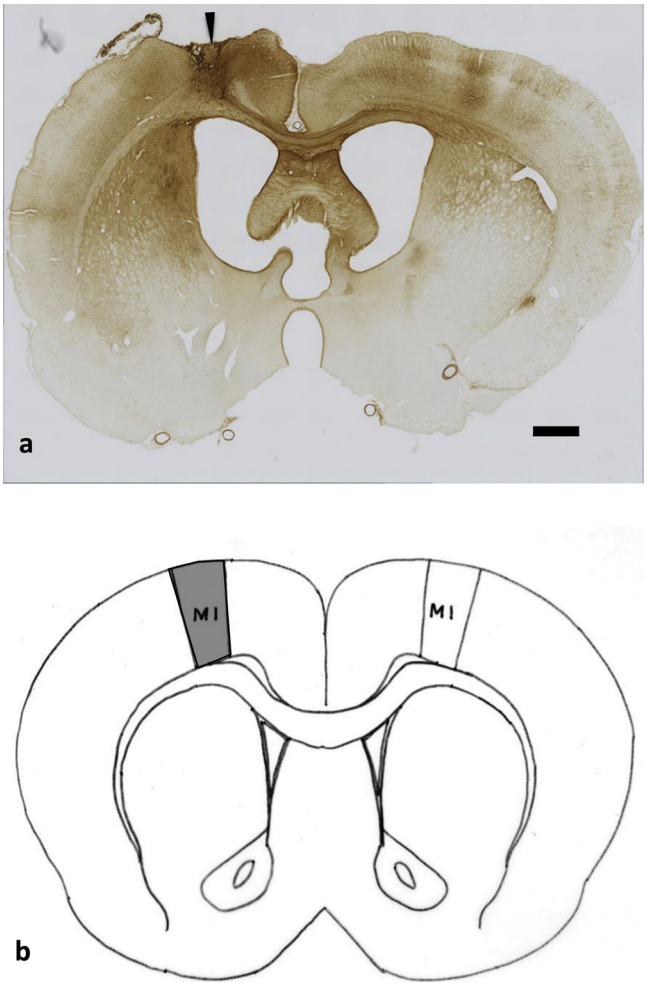


**Fig. 5.** Diagram of injection site. We confirmed that BDA was injected into the cerebral M1 region in all cases. a: Photomicrograph of specimen in brain(black arrow head: injection site)(Scale bar = 1 mm.). b: Diagram of M1(Scale bar = 1 mm).

either side of the parietal region, and measured compound muscle action potentials (CMAP) in the biceps and triceps on both sides. Four consecutive stimuli were delivered with an interstimulus interval of 2 ms and a stimulus intensity of 50 mA, confirming that CMAPs had been abolished ipsilateral to the hemisection. For postoperative analgesia, buprenorphin (0.02 mg/kg; Otuka, Tokyo, Japan) was injected subcutaneously every 12 h for three days. The antibiotic Penicillin G (22,000units/kg; Trauma, Tokyo, Japan) was injected intramuscularly every 24 h for three days. The hemisected rats completed a six weeks behavioral assessment using the New Rating Scale by Martinez et al (Martinez et al., 2009).and were used in further experiments at 24-weeks-old rats (360–430 g), when their forelimb motor function recovery had reached a steady state. The uninjured Control group consisted of 24-week-old rats (360–430 g). Biotinylated dextran amine (BDA: 10.000 MW, Molecular Probes, Inc., Eugene, USA) was used as a neuro-tracing to examine the corticospinal tract.

*Neuro-tracing*

We chose five injection sites in the primary motor cortex (M1), using "The Rat Brain (Paxinos and Charles Watson, 2007)" as a guide with Bregma as the zero point (Fig. 3a). Rats were anesthetized with intraperitoneal xylazine (0.1 mg/kg) and ketamine (3.6 mg/kg), and their heads were fixed in a stereotaxic apparatus. An approximately 3 cm incision was made in the scalp and Bregma was located.

For the injection of BDA to the Control group, four rats received the injection from the left side, and the other four rats received from the right side.

A hand drill was used to make holes in the skull above the injection sites. Glass microinjection needles with 60 μm–100 μm diameter tips were made from glass capillary tubes (3.0 mm diameter: Narishige) using a micropipette puller, and attached to a Hamilton syringe (10 μl, Hamilton, Reno, USA) with a tubing extension. The glass needle was attached to the tubing with epoxy. The needle was inserted into the forebrain, and 10% BDA was injected at a rate of 0.06 μl/min for 13 min using a microsyringe pump (EP-60: Eicom, Kyoto, Japan). The needle was inserted to a depth of 2.0 mm from the surface of the skull and raised 0.4 mm every 13 min to deliver a total of four injections to each site, for a total injection volume of 7.8 μl. Antibiotics and analgesics were administered postoperatively.

*Sacrifice*

Two weeks after BDA injection, rats were deeply anesthetized with an intraperitoneal injection of pentobarbital sodium (50 mg/kg) and transcardially perfused with PBS (0.9%NaCl + 0.1 M phosphate buffer) followed by 400 ml of 4% paraformaldehyde fixative in buffer solution.

*Specimen preparation and photography*

After fixation, the brain and whole spinal cord were removed, and 50 μm consecutive cryosections were prepared from the telencephalon, the medulla cephalad to the pyramidal decussation, the medulla caudal to the pyramidal decussation, the cervical spinal cord cephalad to the hemisection and the cervical spinal cord caudal to the hemisection. The floating sections underwent a chromogenic reaction with diaminobenzidine (DAB: VECTASTAIN Elite ABC Kit, Vector, Burlingame, USA) and mounted on glass slides as specimens (Fig. 3b) (Imai and Aoki, 1993; Nunomaki, 2001; Sakakibara et al., 2008).

Specimens were photographed using a BZ-X710 (KEYENCE, Osaka, Japan).

*Quantitative analysis of imaging data (1)*

An area with the appearance of nerve fibers was categorized to ipsi lateral side (hereinafter referred to as ipsi) or contralateral side (hereinafter referred to as contra) of the Control group or the Hemisection group and recorded by referring all specimen to "The rat brain (Paxinos and Charles Watson, 2007)" for every level.

*Quantitative analysis of imaging data (2)*

Images were analyzed in ImageJ (Rasband, 2014). Images were opened from ImageJ's File menu (Fig. 4a). To separate the hematoxylin and BDA immunostaining from the original sample image, RGB color separation was performed by selecting the H DAB vector in the Color Deconvolution plugin (Fig. 4b). The setting of the color threshold was objectively quantified with reference to the method of Suemitsu et al. (Suemitsu et al., 2012). After RGB color separation, the color thresholds were set with Image > Adjust > Threshold, so that only the DAB-immunostained fibers could be colored (Fig. 4c). Since the staining also

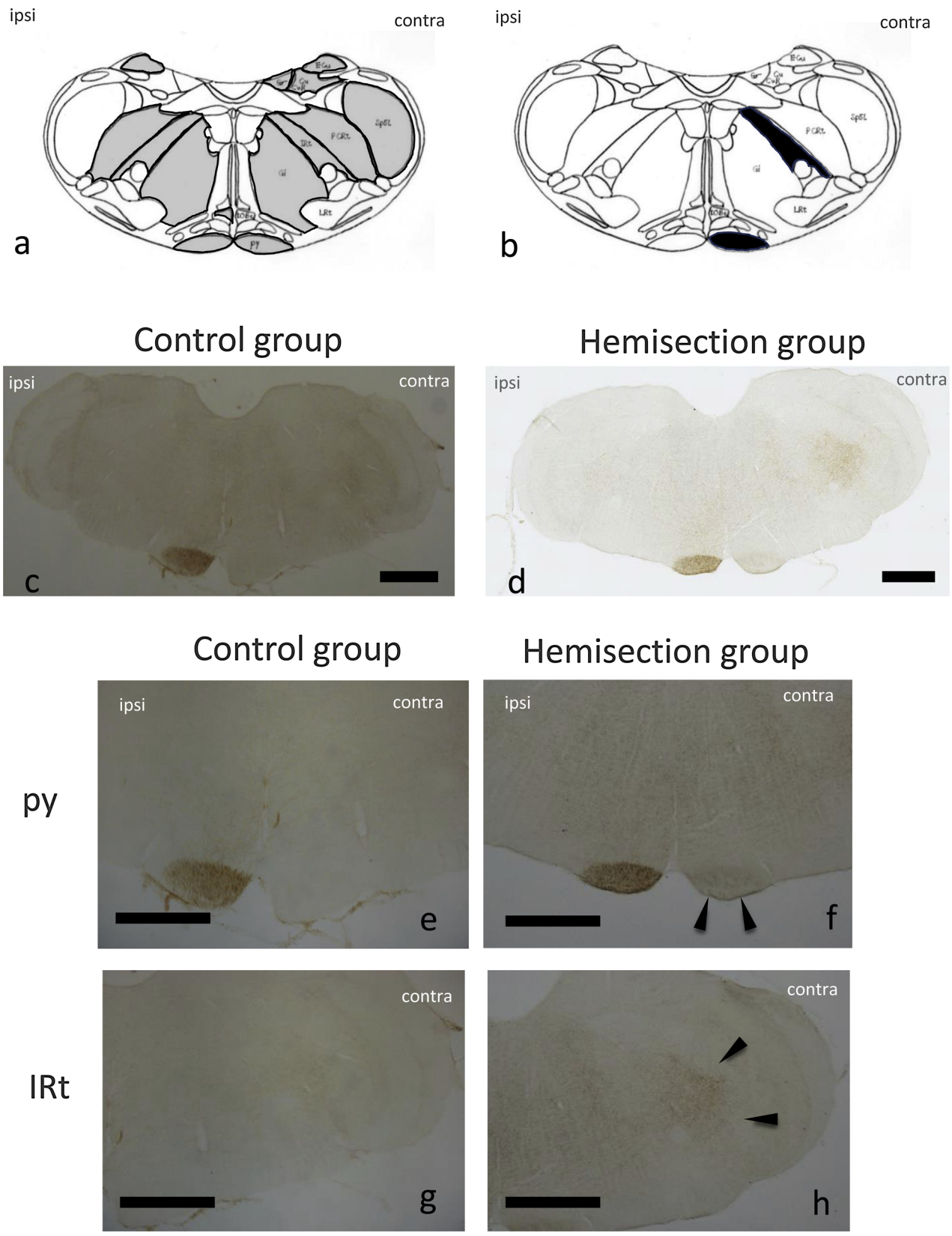


**Fig. 6.** Imaging data analysis (1) for the Medulla cephalad to the pyramidal decussation. a: Nerve fibers were observed in py, IRt, PCRt, Ecu, IoBe, and Gr in ipsi; py, IRt, PCRt, Ecu, Cu, Gi, and SP5I in contra (gray area). b: In the contra of the Hemisection group, nerve fibers tend to be more in py ($p = 0.059$) and IRt ($p = 0.100$) (black area). c: photomicrograph of Control group(Scale bar = 1 mm). d: photomicrograph of Hemisection group (Scale bar = 1 mm). e: photomicrograph of Control group py(Scale bar = 1 mm). f: photomicrograph of Hemisection group py(arrow head : aberrant nerve fibers) (Scale bar = 1 mm). g: photomicrograph of Control group IRt (Scale bar = 1 mm). h: photomicrograph of Hemisection group IRt (arrow head: aberrant nerve fibers). py: pyramidal tract. IRt: intermediate reticular nucleus. PCRt: parvicellular reticular nucleus. Ecu: external cunate nucleus. IoBe: inferior olive subnucleus B of medial nucleus. Gr: gracile nucleus. Cu: cunate nucleus. Gi: gigantcellular reticular nucelus. SP5I: spinal trigeminal nucleus interpolar part (Scale bar = 1 mm).

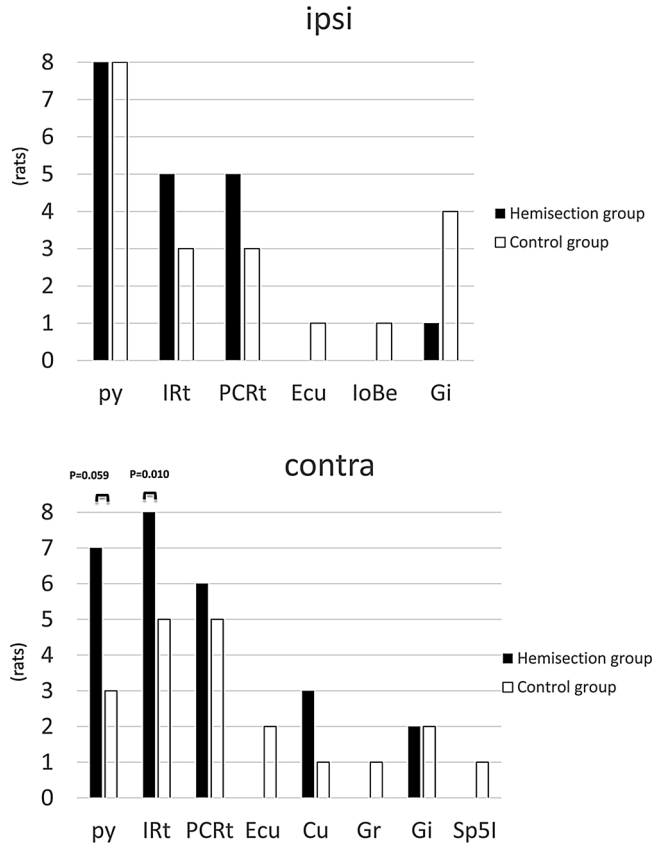


**Fig. 7.** Analysis using Fisher's exact test for the medulla cephalad to the pyramidal decussation In the contra of the Hemisection group, nerve fibers tend to be more in py (p = 0.059) and IRt (p = 0.100).

**Table 1**
Analysis using Fisher's exact test for the medulla cephalad to the pyramidal decussation. Tend to be high in py (p = 0.059) and IRt (p = 0.100) in the contra of the Hemisection group.

| ipsi | Control group (rats) | Hemisection group (rats) | P value (*p < 0.05) |
|---|---|---|---|
| py | 8 | 8 | 1.000 |
| IRt | 3 | 5 | 0.310 |
| PCRt | 3 | 5 | 0.310 |
| Ecu | 1 | 0 | 0.500 |
| IoBe | 1 | 0 | 0.500 |
| Gi | 4 | 1 | 0.141 |
| **contra** | **Control group (rats)** | **Hemisection group (rats)** | **P value (*p < 0.05)** |
| **py** | **3** | **7** | **0.059** |
| **IRt** | **5** | **8** | **0.100** |
| PCRt | 5 | 6 | 0.500 |
| Ecu | 2 | 0 | 0.233 |
| Cu | 1 | 3 | 0.285 |
| Gr | 1 | 0 | 0.500 |
| Gi | 2 | 2 | 0.715 |
| Sp5I | 1 | 0 | 0.500 |

labeled structures which were clearly not nerve fibers, such as the pia mater, we trimmed the images with the polygon selection tool to include only the areas where nerve fibers were stained (Fig. 4d). After this, we used Analyse > Analyse Particles > Summarize to calculate the Total Area positive for immunostaining (Fig. 4e).

To quantify the nerve fibers which crossed the midline, we determined the area which stained positive for BDA on the ipsi and contra, and defined the increase rate of the immunostaining area as (immunostaining positive area of contra/ immunostaining positive area of ipsi) ×100(%)

*Statistical analysis of imaging data (1)*

The area positive with nerve fiber in each level was compared between the Control group and the Hemisection group. Statistical analysis was performed using Fisher's exact test with a p-value less than 0.05 as significant, and 0.05 ≤ p ≤ 0.10 as not significant but have a tendency. Data are represented as mean ± SD.

*Statistical analysis of imaging data (2)*

We compared the specimens and the increase rate of the immunostaining area in the Hemisection group versus the Control group at each level. Mann-Whitney U test was used for the statistical analysis, with p-values less than 0.05 being considered significant. Data are represented as mean ± SD.

## Results

We confirmed that BDA was injected into the cerebral M1 region in all cases (Fig. 5a and b).

*Statistical analysis of imaging data (1)*

*Medulla cephalad to the pyramidal decussation*

The regions where nerve fibers were observed in ipsi: pyramidal tract (py), intermediate reticular nucleus (IRt), parvicellular reticular nucleus (PCRt), external cunate nucleus (Ecu), inferior olive subnucleus B of medial nucleus (IoBe), and gracile nucleus (Gr); in contra: py, IRt, PCRt, Ecu, cunate nucleus (Cu), gigantcellular reticular nucelus (Gi), and spinal trigeminal nucleus interpolar part (SP5I) (Fig. 6a, c and d).

Nerve fibers tend to be observed more in py (p = 0.059) and IRt (p = 0.100) in the contra of the Hemisection group (Figs. 6b, e–h and 7 ) (Table 1).

*Medulla caudal to the pyramidal decussation*

The regions where nerve fibers were observed in ipsi: dorsal corticospinaltract (dcs), laminae 4,5,7,8, lateral spinal nucleus (LSp), lateral cervical nucleus of the spinal cord (LatC), and lateral funicular; in contra: dcs, laminae 4,5,7,8,10, Lsp, LatC, anterior funicular (Fig. 8a, c and d).

Nerve fibers tend to be observed more in laminae 7 (p = 0.059) and laminae 8 (p = 0.100) in ipsi of the Hemisection group (Figs. 8b, e, f and 9 ) (Table 2).

*Cervical spinal cord cephalad to the hemisection*

The regions where nerve fibers were observed in ipsi: dcs, laminae 4–8, Lsp, LatC, and lateral funicular; in contra: dcs, laminae 4–8, Lsp, LatC, and anterior funicular (Fig. 10a, c and d).

Nerve fibers tend to be observed more in laminae 7 (p = 0.059) in contra of the Hemisection group (Figs. 10b, e, f and 11 ) (Table 3).

*Cervical spinal cord caudal to the hemisection*

Nerve fibers were identified in ipsi: laminae 1–8, Lsp, and lateral funicular; in contra: dcs, laminae 7, anterior funicular, and lateral funicular (Fig. 12a, c and d).

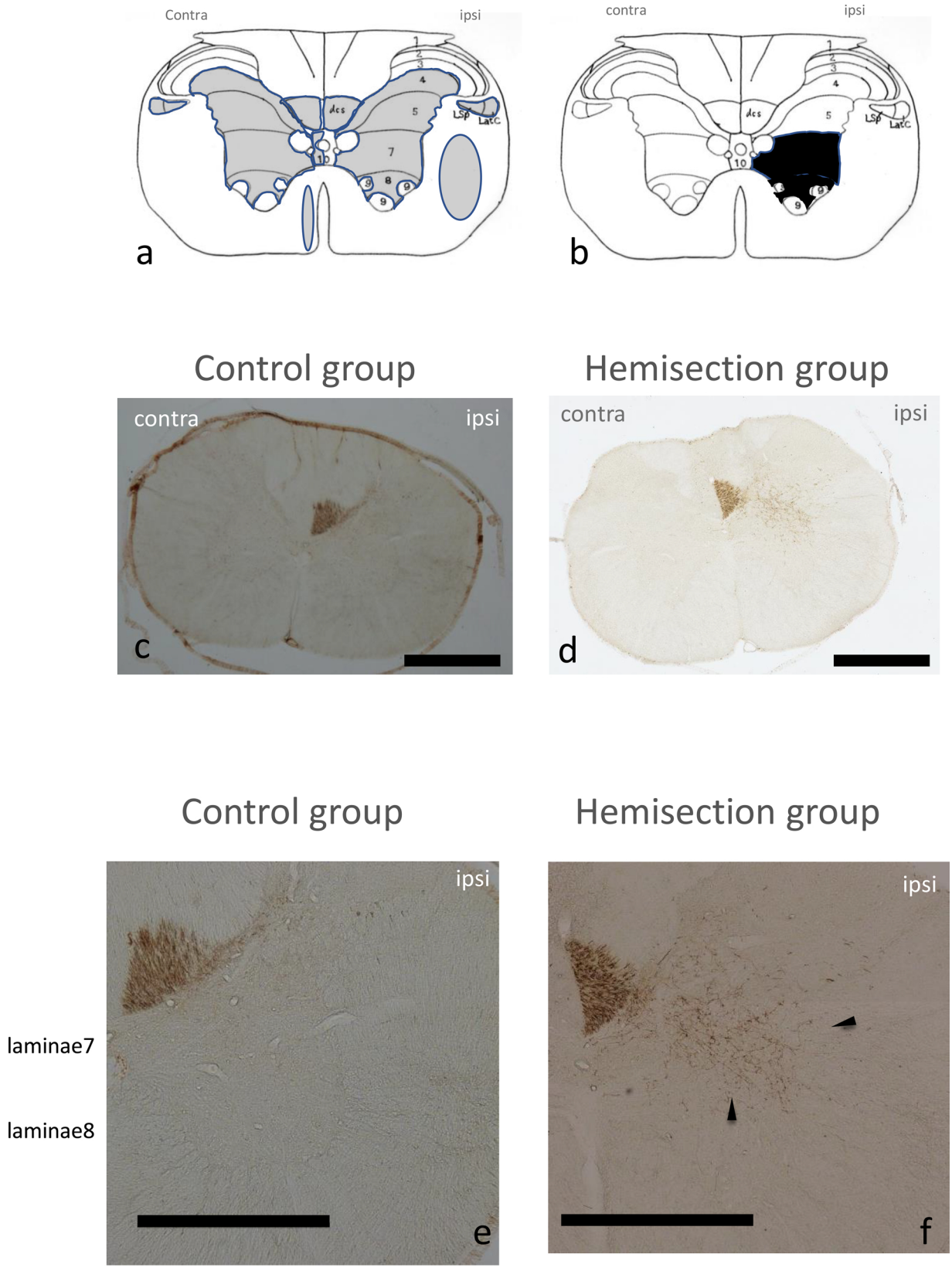


**Fig. 8.** Imaging data analysis (1) for the Medulla caudal to the pyramidal decussation. a: Aberrant nerve fibers were observed in dcs, laminae 4,5,7,8, Lsp, LatC, and lateral funicular in ipsi; dcs, laminae 4,5,7,8,10, Lsp, LatC, and anterior funicular in contra (gray area) (Scale bar = 1 mm). b: In the ipsi of the Hemisection group, aberrant nerve fibers tend to be more in laminae 7 ($p = 0.059$) and laminae 8 ($p = 0.100$) (black area) (Scale bar = 1 mm). c: photomicrograph of Control group (Scale bar = 1 mm). d: photomicrograph of Hemisection group. e: photomicrograph of Control group laminae 7,8. f: photomicrograph of Hemisection group laminae 7,8. (black arrow head : aberrant nerve fibers). dcs: dorsal corticospinal tract. LSp: lateral spinal nucleus. LatC: lateral cervical nucleus of the spinal cord(Scale bar = 1 mm).

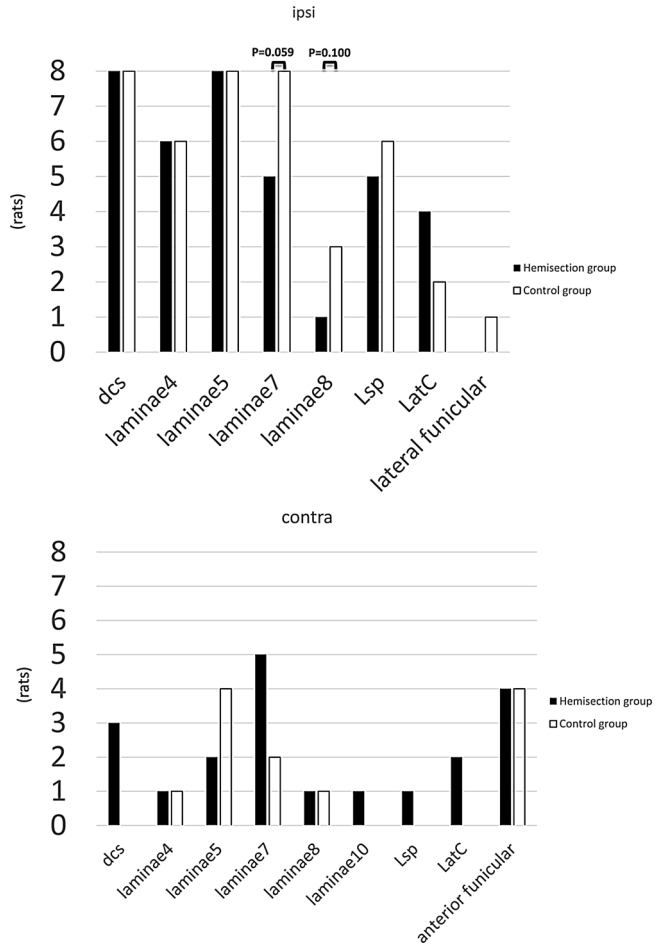


**Fig. 9.** Analysis using Fisher's exact test for the medulla caudal to the pyramidal decussation In the ipsi of the Hemisection group, aberrant nerve fibers tend to be more in laminae 7 (p = 0.059) and laminae 8 (p = 0.100).

**Table 2**
Analysis using Fisher's exact test for the medulla caudal to the pyramidal decussation. Tend to be high in laminae 7 (p = 0.059) and laminae 8 (p = 0.100) in the ipsi of the Hemisection group.

| ipsi | Control group (rats) | Hemisection group (rats) | P value (*P < 0.05) |
|---|---|---|---|
| dcs | 8 | 8 | 1.000 |
| laminae4 | 6 | 6 | 0.715 |
| laminae5 | 8 | 8 | 1.000 |
| laminae7 | **5** | **8** | **0.039*** |
| laminae8 | **1** | **3** | **0.100** |
| Lsp | 5 | 6 | 0.285 |
| LatC | 4 | 2 | 0.500 |
| lateral funicular | 0 | 1 | 0.304 |

| contra | Control group (rats) | Hemisection group (rats) | P value (*P < 0.05) |
|---|---|---|---|
| dcs | 0 | 3 | 0.255 |
| laminae4 | 1 | 1 | 0.761 |
| laminae5 | 4 | 2 | 0.304 |
| laminae7 | 2 | 5 | 0.304 |
| laminae8 | 1 | 1 | 0.767 |
| laminae10 | 0 | 1 | 0.500 |
| Lsp | 0 | 1 | 0.500 |
| LatC | 0 | 2 | 0.200 |
| anterior funicular | 4 | 4 | 0.690 |

In ipsi of the Hemisection group, nerve fibers were significantly more in the lateral funicular (p = 0.039), significantly less in dcs (p < 0.001), laminae 4 (p = 0.020), and laminae 5 (p = 0.020), and had a tendency of less in laminae 7 (p = 0.059) (Fig. 12b, e, f, i and j) (Fig. 13) (Table 4). In contra of the Hemisection group, nerve fibers tend to be more in lateral funicular (p = 0.100) (Figs. 12g, h and 13) (Table 4).

*Statistical analysis of imaging data (2)*

*Medulla cephalad to the pyramidal decussation*

The increase rate of the immunostaining area in the Control group was 54.761 ± 63.280%, and that in the Hemisection group was 82.844 ± 88.021%, which was not significant (P = 0.959) (Fig. 14).

*Medulla caudal to the pyramidal decussation*

The increase rate of the immunostaining area in the Control group was 6.643 ± 6.197%, and that in the Hemisection group was 10.941 ± 15.766%, which was not significant (P = 0.901) (Fig. 15).

*Cervical spinal cord cephalad to the hemisection*

The increase rate of the immunostaining area in the Control group was 13.246 ± 12.402%, and that in the Hemisection group was 14.854 ± 18.997%, which was not significant (P = 0.959) (Fig. 16).

*Cervical spinal cord caudal to the hemisection*

There were few immunostaining-labeled nerve fibers observed in the Hemisection group. Image process was attempted using ImageJ but it was unsuccessful due to a lot of noise. No test of significant difference was performed because the increase rate of the immunostaining area becomes large due to the small area of ipsi in the Hemisection group, thereby the apparent significant difference will be calculated to be large when compared with the increase rate of the immunostaining area in the Control group (Fig. 17).

*Summary of results*

Aberrant nerve fibers were identified in different areas in each level in the Hemisection group compared with the Control group.

Image analysis (1) revealed that the Hemisection group showed more nerve fibers in: py and IRt in the contra of medulla cephalad to pyramidal decussation; laminae 7,8 in the ipsi of medulla caudal to the pyramidal decussation; laminae 7 in the contra of cervical spine cephalad to hemisection; lateral funicular in the ipsi, and lateral funicular in the contra of cervical spine caudal to hemisection, while they were less in: dcs, laminae 4,5,6 in the ipsi of the cervical spine caudal to hemisection.

Meanwhile, image analysis (2) revealed no significant difference in the increase rate of the immunostaining area between the Control group and the Hemisection group.

## Discussion

The rat corticospinal tract begins in M1, passes through the ipsilateral ventral medulla, decussates at the pyramidal decussation, passes through the base of the contralateral dorsal column in the spinal cord, and terminates in the dorsal horn (Imai and Aoki, 1993; Nunomaki, 2001; Martinez et al., 2009). In contrast, the human corticospinal tract runs from M1 through the ipsilateral ventral medulla and decussates at the pyramidal decussation, and from there approximately 80% of the fibers descend in the dorsolateral funicular (Micheal et al., 2009).

The rat and human corticospinal tracts are similar in that both descend from M1 through the ventral medulla and decussate at the

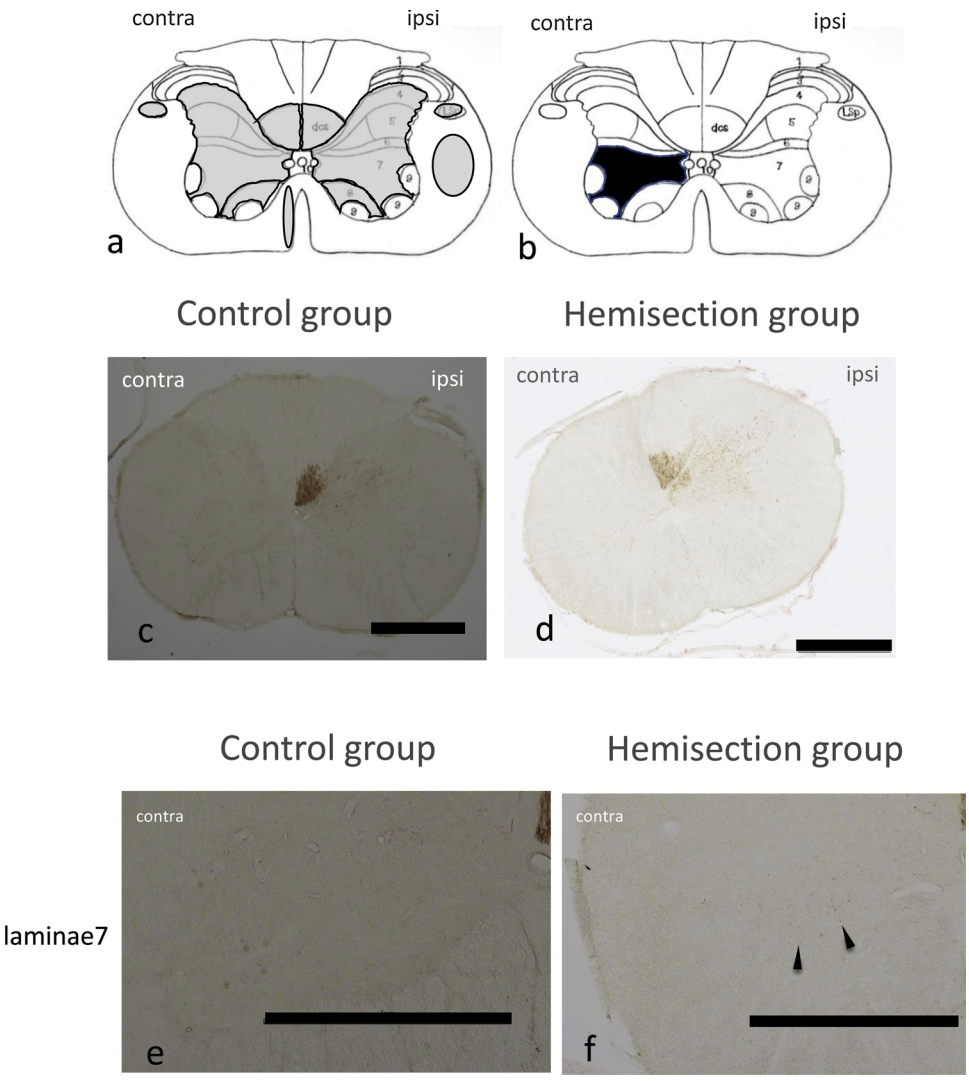


**Fig. 10.** Imaging data analysis (1) for the cervical spinal cord cephalad to the hemisection (Scale bar = 1 mm). a: Nerve fibers were observed in dcs, laminae 4–8, Lsp, LatC, and lateral funicular in ipsi; dcs, laminae 4–8, Lsp, LatC, and anterior funicular in contra (gray area). b: In the contra of the Hemisection group, nerve fibers tend to be more in laminae7 ($p = 0.059$). c: photomicrograph of Control group(Scale bar = 1 mm). d: photomicrograph of Hemisection group(Scale bar = 1 mm). e: photomicrograph of Control group laminae7(Scale bar = 1 mm). f: photomicrograph of Hemisection group laminae7 (black arrow head : aberrant nerve fibers). dcs: dorsal corticospinal tract. LSp: lateral spinal nucleus. LatC: lateral cervical nucleus of the spinal cord(Scale bar = 1 mm).

pyramidal decussation. They differ after the decussation, however, with the rat corticospinal tract descending in the base of the dorsal column and the human descending in the dorsolateral funicular.

In our Control group, the stained pathway was similar to previous reports of the rat corticospinal tract. Accordingly, it is reasonable to conclude that our 5 chosen cortical injection sites were in M1.

In our previous study of circuit remodeling in rats after cervical spinal hemisection, we conducted a longitudinal behavioral assessment in hemisected rats and reported that their motor forelimb motor function deficits improved by 34% (Hasegawa et al., 2016). In this study, we found that the hemisection rats had nerve fibers in the medulla cephalad to pyramidal decussation, the medulla caudal to pyramidal decussation, the C5/6 cervical spinal cord which were not present in the control rats. We used the following strategies to prove that these new fibers are involved in the forelimb motor function restoration. When preparing our cervical spinal hemisection models, we excised a 2 mm segmental hemisection because simply cutting with a sharp scalpel would make it possible for nerve fibers to regrow after the injury where the severed spinal cord halves contact each other. As a result, when we injected BDA into the right M1 in the Hemisection group, we saw no staining at the base of the dorsal column caudal to the lesion, allowing us to eliminate the possibility that the hemisected nerve fibers had regenerated. We used CMAPs to check whether any of the spinal cord was left uncut during the hemisection. At the time of the hemisection, we confirmed that electrical potentials were completely lost from the damaged side, and that the rat's forelimb exhibited total flaccid paralysis after the injury. This eliminates the possibility that the hemisection was incomplete.

In an effort to objectively assess the percent increase in immunostained nerve fibers in the Control group and the Hemisection group, we used ImageJ (Paxinos and Charles Watson, 2007) to quantify their nerve fibers. Because we felt it would be difficult to eliminate the effects of ambiguity and cognitive biases using the method developed by Suemitsu et al (Suemitsu et al., 2012) in which the labeled nerve fibers in immunostained tissue samples are directly counted visually, we used ImageJ to quantify the specimens. We introduced a method for

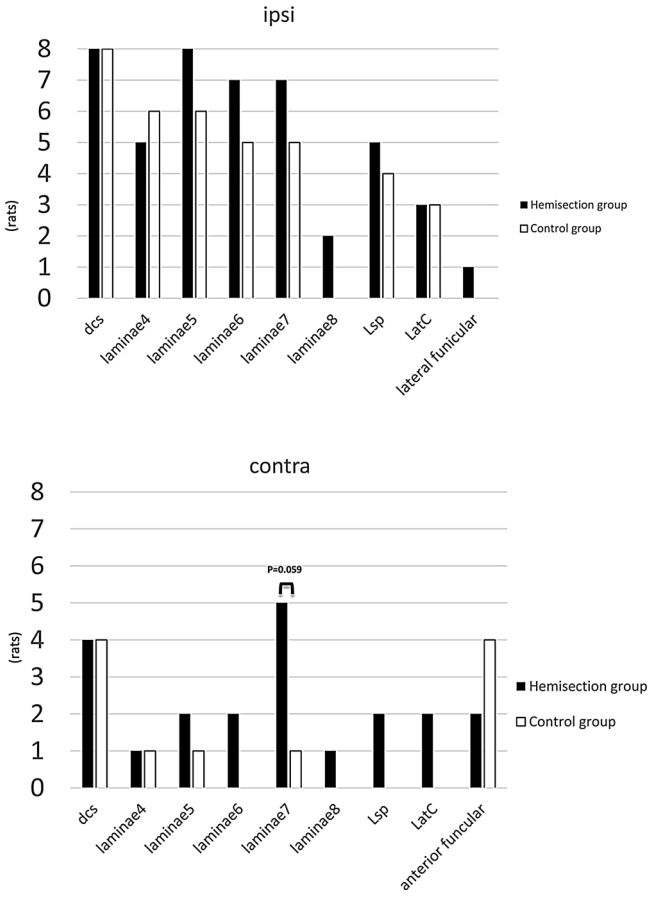


**Fig. 11.** Analysis using Fisher's exact test for the cervical spinal cord cephalad to the hemisection.
In the contra of the Hemisection group, nerve fibers tend to be more in laminae 7 (p = 0.059).

**Table 3**
Analysis using Fisher's exact test for the cervical spinal cord cephalad to the hemisection. Tend to be high in laminae 7 (p = 0.059) in the contra of the Hemisection group.

| ipsi | Control group (rats) | Hemisection group (rats) | P value (*p < 0.05) |
|---|---|---|---|
| dcs | 8 | 8 | 1.000 |
| laminae4 | 6 | 5 | 0.467 |
| laminae5 | 6 | 8 | 0.233 |
| laminae6 | 5 | 7 | 0.285 |
| laminae7 | 5 | 7 | 0.285 |
| laminae8 | 0 | 2 | 0.233 |
| Lsp | 4 | 5 | 0.500 |
| LatC | 3 | 3 | 0.696 |
| lateral funicular | 0 | 1 | 0.500 |
| **contra** | **Control group (rats)** | **Hemisection group (rats)** | **P value (*p < 0.05)** |
| dcs | 4 | 4 | 0.690 |
| laminae4 | 1 | 1 | 0.767 |
| laminae5 | 1 | 2 | 0.500 |
| laminae6 | 0 | 2 | 0.233 |
| **laminae7** | **1** | **5** | **0.059** |
| laminae8 | 0 | 1 | 0.500 |
| Lsp | 0 | 2 | 0.233 |
| LatC | 0 | 2 | 0.233 |
| anterior funcular | 4 | 2 | 0.304 |

objectively assessing the data by calculating the proportions of each component. We also quantified the BDA-labeled nerve fibers using a method based on that of Suemitsu et al., and defined an increase rate of the immunostaining area, which we compared between the Control group and the Hemisection group. Although no significant difference was noted in our study, the method has the potential to be a useful quantitative evaluation if the evaluation is limited to a certain area.

There are a number of previous reports on the recovery of motor function following spinal cord injury. In a 2012 experiment by Van Den Brand et al. (2012), rats were subjected to hemisection at different levels (T7 and T10) on each side of the thoracic spinal cord, resulting in a complete interruption of direct descending pathways from the upper central nervous system. After the injury, plasticity was induced by making the rats perform voluntary movements, and a neuroanatomical assessment was conducted via neuro-tracing with BDA. There was an increase in corticospinal tract branching and propriospinal neurons in the gray matter of the intermediate lamina on the injured side at the T8/T9 level. The location of the injury in this experiment differs from ours, but the results were similar in terms of the type of lesion (hemisection) and the fact that new nerve fibers were seen caudal to the lesion after the injury.

Freund et al. and Rosenzweig et al. performed cervical spinal hemisection from C7 to C8 in macaques, and showed that the corticospinal tract sends projections from the uninjured side across midline to the injured side caudal to the lesion (Freund et al., 2007; Rosenzweig et al., 2010).

Using a macaque model in which the pyramidal tracts were selectively lesioned at C4/5, Alstermark et al. and Isa et al. reported that many axon collaterals from the corticospinal tract projected into the gray matter of the intermediate laminae at various levels both rostral and caudal to the lesion (Alstermark et al., 1999; Alstermark and Isa, 2012; Isa, 2006). Although these experiments used a different species, their results are consistent with ours in that they found the cerebrospinal tract from the healthy side crossing over the midline into the injured side.

It has been demonstrated that propriospinal neuron involves the recovery of exquisite motor function of the forelimb in macaque spinal cord injury model (Alstermark and Pettersson, 2014; Tohyama et al., 2017) and the neuron resides in the gray matter of C3/4 segment (laminae6-7). An evidence that the propriospinal neuron contributes to the recovery of forelimb function following spinal cord injury has been shown also in the feline experiment (Alstermark et al., 2011). In our rat study also, an increase in the aberrant nerve fiber was noted in the gray matter of the Hemisection group. Therefore the propriospinal neuron might have contributed to the forelimb motor function restoration in the Hemisection group.

Many presentations have pointed out the involvement of the reticulospinal tract in the motor function compensatory pathway following spinal cord injury. In 2014, Alstermark et al. described that, when the lesion is not so extensive and the continuity of the neural circuit remains to some extent, the cerebellar loop including reticulospinal, rubrospinal, and corticospinal tracts regulates the enhancement of synaptic transmission from unlesioned side pathway, and the cerebellar loop is involved in motor function restoration (Alstermark and Pettersson, 2014).

Zörner et al. and Filli et al. also mentioned the involvement of the reticulospinal tract in the mesencephalic locomotor region in 2014 (Filli et al., 2014; Zörner et al., 2014). Furthermore, Esposito et al. reported that brainstem nucleus medullary reticular formation ventral part involves forelimb motor tasks in 2014 (Esposito et al., 2014). Filli et al.

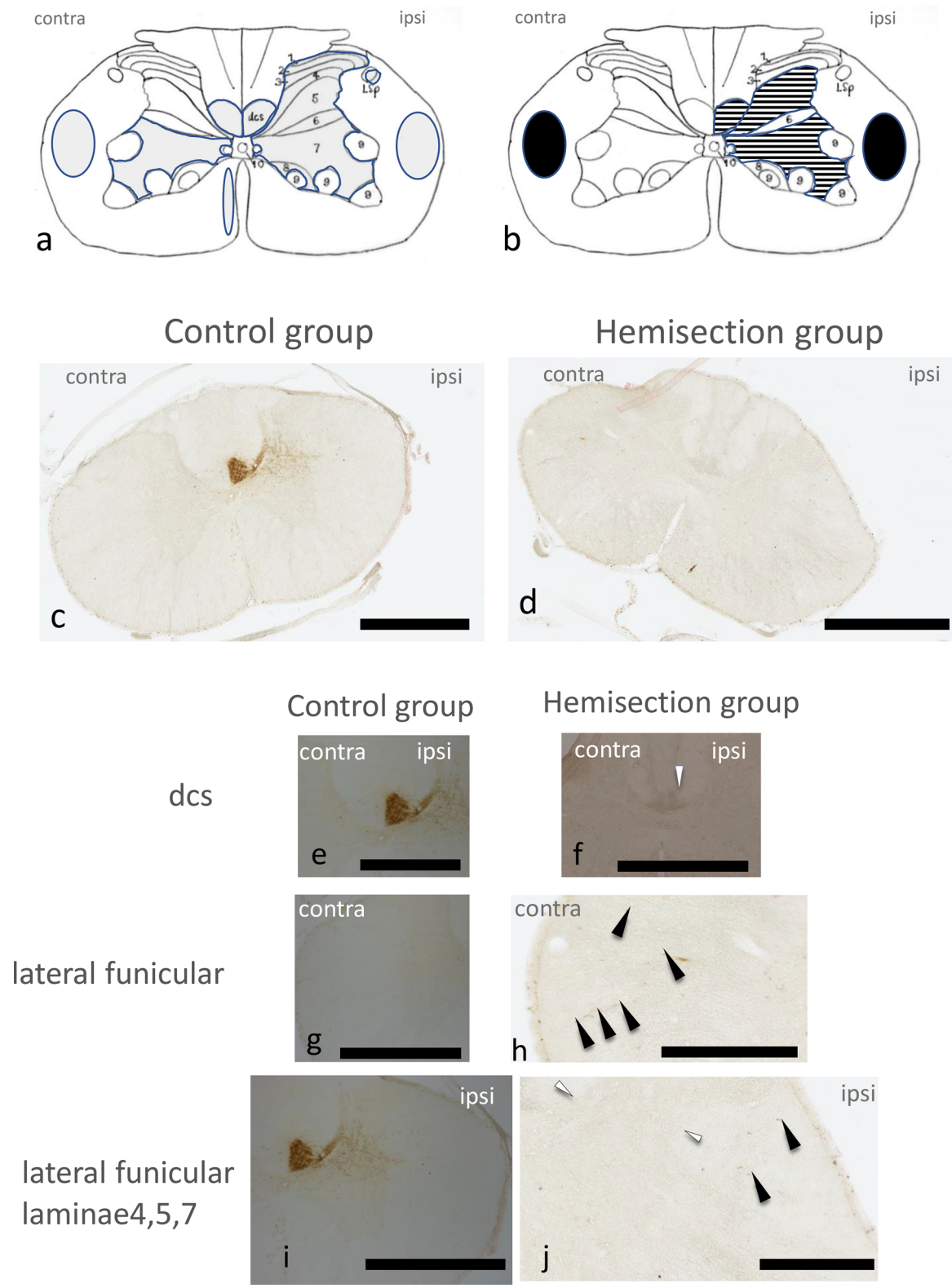


**Fig. 12.** Imaging data analysis (1) for the cervical spinal cord caudal to the hemisection (Scale bar = 1 mm). a: Nerve fibers were observed in dcs, laminae 1,2,3,4,5,6,7,8, Lsp, and lateral funicular in ipsi; dcs, laminae 7, anterior funicular, and lateral funicular in contra (gray area). b: In the ipsi of the Hemisection group, nerve fibers were significantly more in lateral funicular ($p = 0.039$), significantly less in dcs ($p < 0.001$), laminae 4 ($p = 0.020$), and laminae 5 ($p = 0.020$), and tend to be less in laminae 7 ($p = 0.059$). In the contra of the Hemisection group, nerve fibers tend to be high in lateral funicular ($p = 0.100$) (black area: increased parts) (stripe area: decreased parts) c: photomicrograph of Control group (Scale bar = 1 mm). d: photomicrograph of Hemisection group. e: photomicrograph of Control group contra dcs(Scale bar = 1 mm). f: Photomicrograph of dcs in the contra of the Hemisection group. (white arrow head: nerve fibers decreased compared with the Control group or unknown) (Scale bar = 1 mm). g: photomicrograph of Control group lateral funicular. h: photomicrograph of Hemisection group lateral funicular (black arrow head: aberrant nerve fibers) (Scale bar = 0.5 mm). i: photomicrograph of Control group lateral funicular(ipsi), lateral funicular, laminae4,5,7 (Scale bar = 1 mm). *j*: photomicrograph of Hemisection group lateral funicular(ipsi), lateral funicular, laminae4,5,7 (black arrow head: aberrant nerve fibers) (white arrow head: nerve fibers decreased compared with the Control group or unknown). dcs: dorsal corticospinal tract (Scale bar = 0.5 mm.).

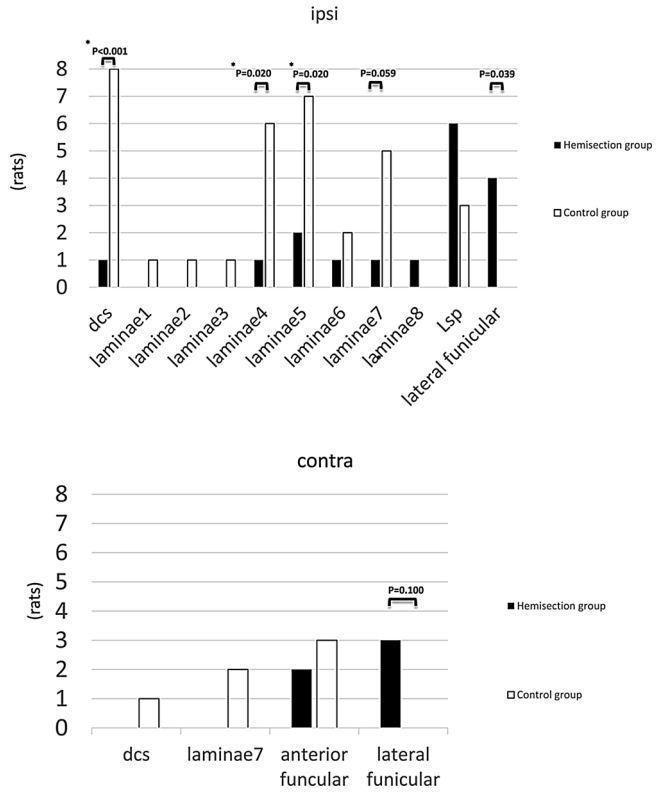


**Fig. 13.** Analysis using Fisher's exact test for the cervical spinal cord caudal to the hemisection.
It was significantly high in lateral funiculus (p = 0.039) in the ipsi of the Hemisection group, significantly low in dcs (p < 0.001), laminae 4 (p = 0.020), and laminae 5 (p = 0.020), and it tends to be low in laminae 7 (p = 0.059) (* p < 0.05).

**Table 4**
Analysis using Fisher's exact test for the cervical spinal cord caudal to the hemisection. Significantly high in lateral funiculus (p = 0.039), significantly low in dcs (p < 0.001), laminae 4 (p = 0.020), and laminae 5 (p = 0.020), tend to be low in laminae 7 (p = 0.059) in the ipsi of the Hemisection group. Tend to be high in lateral funiculus (p = 0.100) in the contra of the Hemisection group.

| ipsi | Control group (rats) | Hemisection group (rats) | P value (*p < 0.05) |
|---|---|---|---|
| dcs | **8** | **1** | **0.001*** |
| laminae1 | 1 | 0 | 0.500 |
| laminae2 | 1 | 0 | 0.500 |
| laminae3 | 1 | 0 | 0.500 |
| laminae4 | **6** | **1** | **0.020*** |
| laminae5 | **7** | **2** | **0.020*** |
| laminae6 | 2 | 1 | 0.500 |
| laminae7 | **5** | **1** | **0.059** |
| laminae8 | 0 | 1 | 0.500 |
| Lsp | 3 | 6 | 0.157 |
| LatC | 1 | 1 | 0.767 |
| lateral funicular | **0** | **4** | **0.039*** |

| contra | Control group (rats) | Hemisection group (rats) | P value (*p < 0.05) |
|---|---|---|---|
| dcs | 1 | 0 | 0.500 |
| laminae7 | 2 | 0 | 0.233 |
| anterior funcular | 3 | 2 | 0.500 |
| lateral funicular | **0** | **3** | **0.100** |

and Zörner et al. found an increase in nerve fiber to the ipsilesional gigantocellular reticular nucleus in a neuro-tracing experiment of cervical spinal spinal cord hemisection rat (C4 level), and demonstrated the substantial regenerative fiber sprouting of reticulospinal axons located above the lesion.

They described the result was due to a compensation route change at advanced control level such as the arborization of reticulospinal fibers and detouring the lesion by the contact with C3/4 propriospinal neuron and the contribution of the rostral side nerve fibers crossing the midline on the intact side to the motor function restoration. Our results demonstrated a tendency of an appearance of nerve fibers in IRt in the medulla cephalad to pyramidal decussation, therefore it may reflect these previous reports.

Meanwhile, Weishaupt et al. conducted a nerve tracer experiment in spinal cord injury rat model (hemisection of C4 level dorsal corticospinal tract) and found that a significant decrease in the corticospinal tract sprouting and reticulospinal tract fiber density. They thought that the corticospinal tract rewriting alone cannot sufficiently explain motor function recovery demonstrated by behavioral experiment and speculated the involvement of a mechanism other than the anatomical plasticity or the plasticity change at the cellular level(Weishaupt et al., 2013). In accord with their result, a decrease in the nerve fibers on the hemisected caudal side was observed in our experiment.

Umeda et al. demonstrated that the nerve fibers from ipsi contribute to the compensatory process of motor function by a neuro-tracer experiment in rat brain-injured model and described the compensatory process differs in the rostral side and caudal side (Umeda et al., 2010; Umeda and Isa, 2011).

Similarly, Ueno et al. demonstrated that spontaneous recovery after injury in brain-injured mice constructs a compensatory neural network with comprising spinal interneuron and propriospinal neuron (Ueno et al., 2012).

At the cerebral level, Nishimura et al and Kinoshita et al reported that functional binding of ventral striatum including nucleus accumbens with M1 is selectively elevated during the recovery period in the macaque spinal cord injury model (Kinoshita et al., 2012; Nishimura et al., 2011).

It is believed that these nerve fibers, which are not present in healthy animals, are involved in the partial recovery of function after spinal cord injury. We also observed nerve fibers crossing the midline from the undamaged side to the damaged side in rats which recovered forelimb motor function after cervical spinal cord hemisection, and we believe these fibers are involved in improved forelimb motor function. (Fig. 18).

## Conclusion

In rats that recovered forelimb motor function after cervical spinal cord hemisection, nerve fibers from the corticospinal tract crossed the midline from the ipsi lateral side to the contra lateral side in the each levels. There is a high probability that these aberrant nerve fibers beyond the midline from the undamaged side to the damaged side could be involved in forelimb motor function restoration in rats with cervical cord hemisection.

## Conflict of interest

The authors declare no conflict of interest.

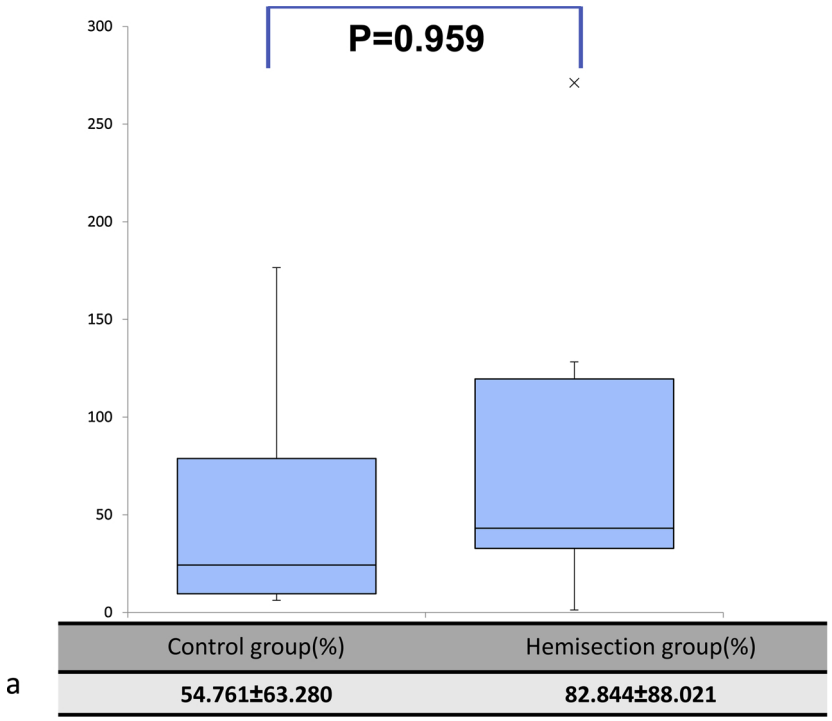


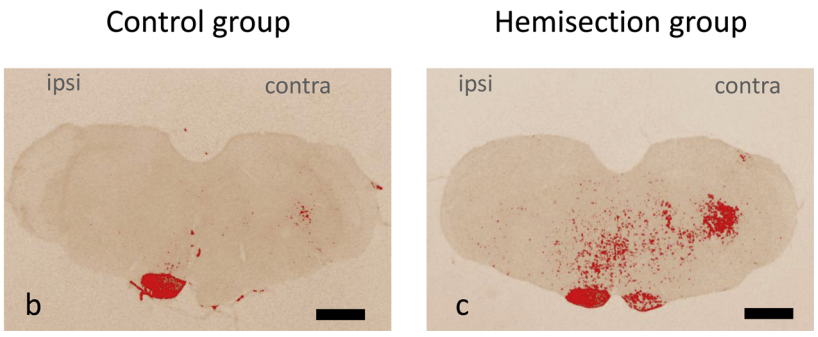


**Fig. 14.** Imaging data analysis (2) for the medulla cephalad to the pyramidal decussation. a: Analysis of immunostaining area using Mann-Whitney U test. Increase rate of the immunostaining area in the Control group was 54.761 ± 63.280%, that in the Hemisection group was 82.844 ± 88.021% with no significant difference (P = 0.959). b: Image of the Control group after the analysis using ImageJ (Scale bar = 1 mm). c: Image of the Hemisection group after the analysis using ImageJ (Scale bar = 1 mm).

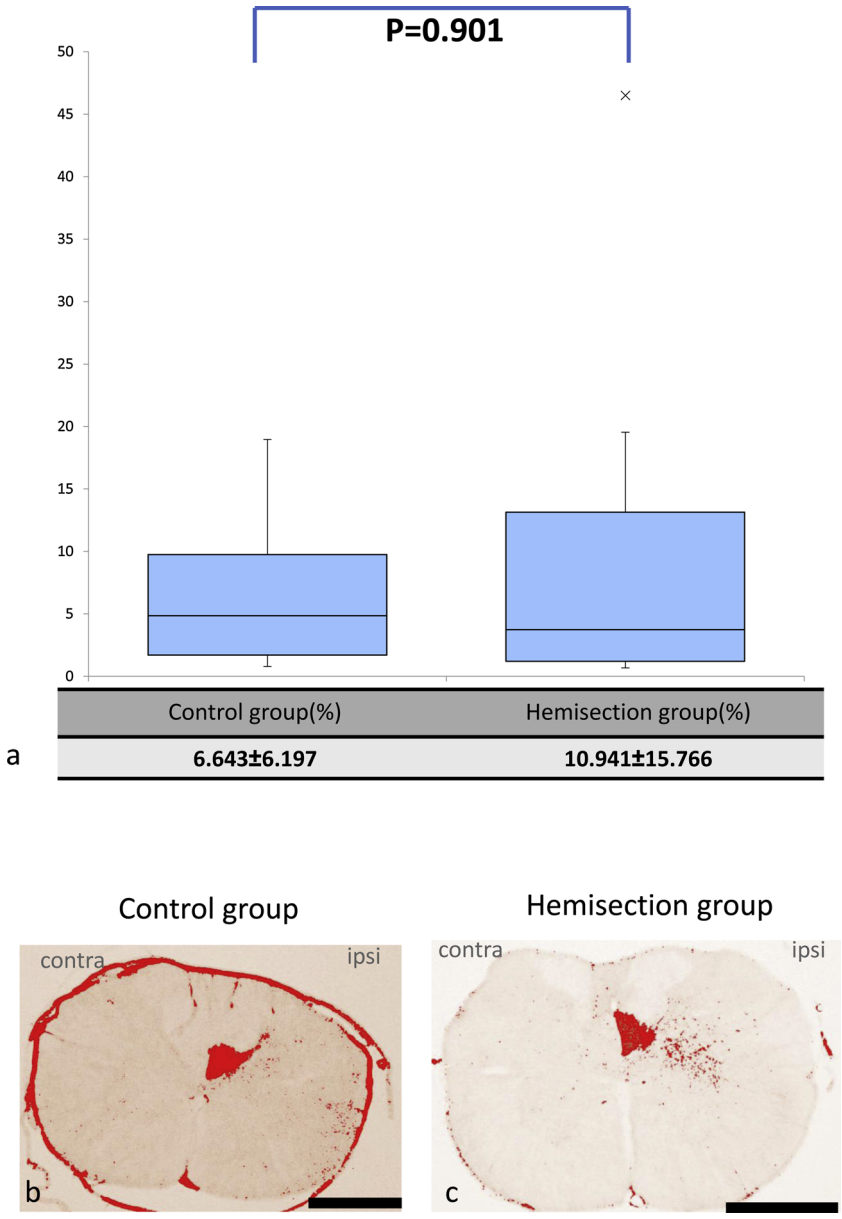


**Fig. 15.** Imaging data analysis (2) for the medulla caudal to the pyramidal decussation (Scale bar = 1 mm). a: Analysis of immunostaining area using Mann-Whitney U test. Increase rate of the immunostaining area in the Control group was 6.643 ± 6.197%, that in the Hemisection group was 10.941 ± 15.766% with no significant difference (P = 0.901). b: Image of the Control group after the analysis using ImageJ (Scale bar = 1 mm). c: Image of the Hemisection group after the analysis using ImageJ (Scale bar = 1 mm).

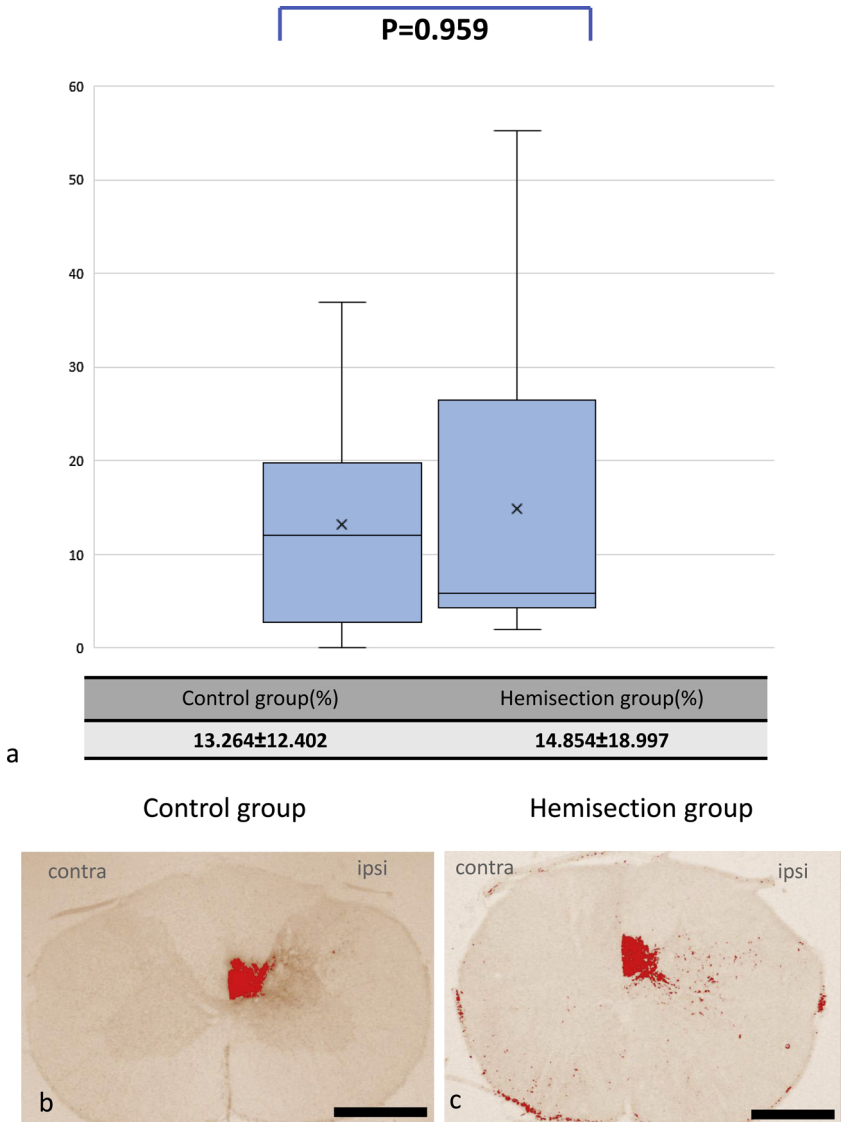


**Fig. 16.** Imaging data analysis (2) for the cervical spinal cord cephalad to the pyramidal decussation (Scale bar = 1 mm. a: Analysis of immunostaining area using Mann-Whitney U test. Increase rate of the immunostaining area in the Control group was 13.264 ± 12.402%, that in the Hemisection group was 14.854 ± 18.997% with no significant difference (P = 0.959). b: Image of the Control group after the analysis using ImageJ (Scale bar = 1 mm). c: Image of the Hemisection group after the analysis using ImageJ (Scale bar = 1 mm).

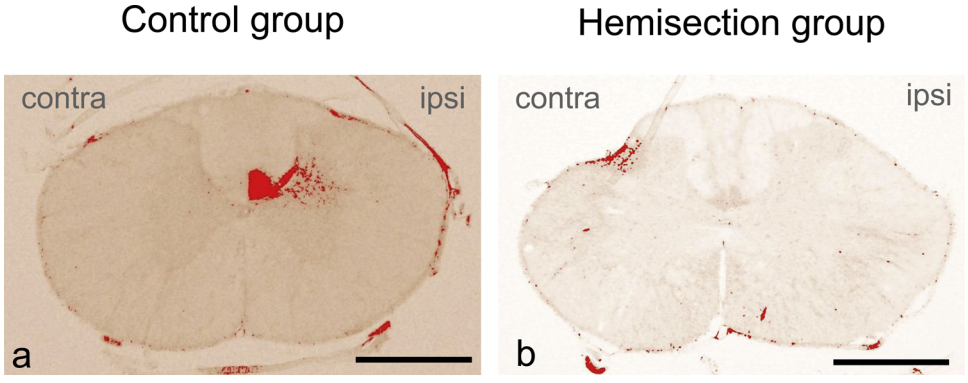


**Fig. 17.** Imaging data analysis (2) for the cervical spinal cord caudal to the hemisection. There were few immunostaining-labeled nerve fibers observed in the Hemisection group. Image process was attempted using ImageJ but it was unsuccessful due to a lot of noise. No test of significant difference was performed because the increase rate of the immunostaining area becomes large due to the small area of ipsi in the Hemisection group, thereby the apparent significant difference will be calculated to be large when compared with the increase rate of the immunostaining area in the Control group. a: Image of the Control group after the analysis using ImageJ (Scale bar = 1 mm). b: Image of the Hemisection group after the analysis using ImageJ (Scale bar = 1 mm).

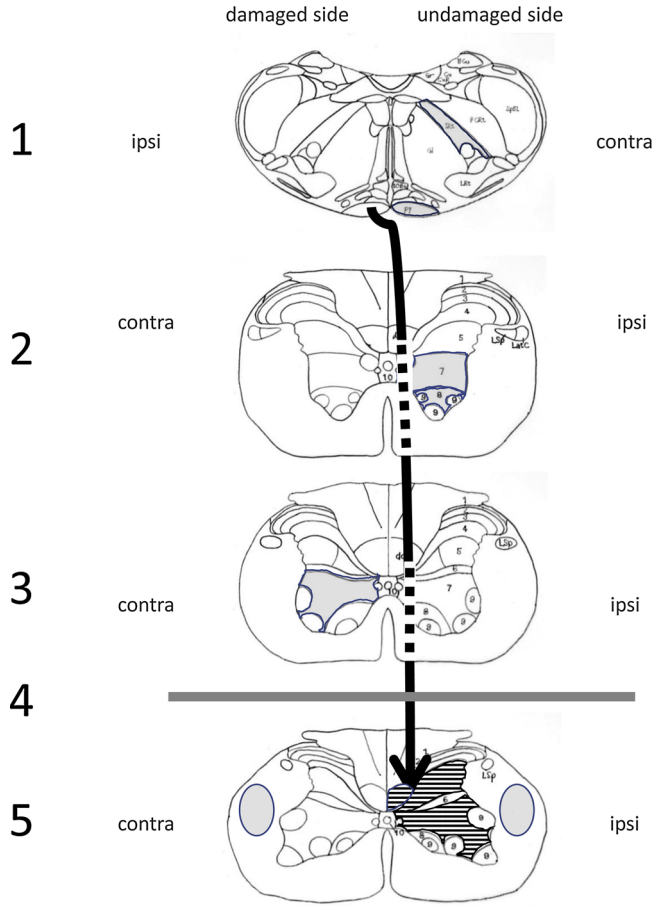


**Fig. 18.** Diagram of a candidate mechanism of the forelimb motor function restoration in rats with cervical spinal cord hemisection. We observed nerve fibers crossing the midline from the ipsi to the contra in rats which recovered forelimb motor function after cervical spinal cord hemisection, and we believe these fibers are involved in improved forelimb motor function. gray area: increase parts. stripe area: decrease parts. black arrow: corticospinal tract. (1) Medulla cephalad to pyramidal decussation. (2) Medulla caudal to pyramidal decussation. (3) Cervical spinal cord cephalad to the hemisection. (4) Hemisection site. (5) Cervical spinal cord caudal to the hemisection.

## Acknowledgements

The authors thank Ms. Mizuho Kosuge for her assistance with this study. This work was supported by a grant from the Japan Orthopaedics and Traumatology Foundation, Inc. (no. 252).

## References

Alstermark, B., Isa, T., Ohki, Y., Saito, Y., 1999. Disynaptic pyramidal excitation in forelimb motoneurons mediated via C(3)-C(4) propriospinal neurons in the Macaca fuscata. J. Neurophysiol. 82 (6), 3580–3585. https://doi.org/10.1152/jn.1999.82.6.3580.

Alstermark, B., Pettersson, L.G., Nishimura, Y., Yoshino-Saito, K., Tsuboi, F., Takahashi, M., Isa, T., 2011. Motor command for precision grip in the macaque monkey can be mediated by spinal interneurons. J. Neurophysiol. 106 (1), 122–126. https://doi.org/10.1152/jn.00089.2011.

Alstermark, B., Isa, T., 2012. Circuits for skilled reaching and grasping. Annu. Rev. Neurosci. 35, 559–578. https://doi.org/10.1146/annurev-neuro-062111-150527.

Alstermark, B., Pettersson, L.G., 2014. Endogenous plasticity in neuro-rehabilitation following partial spinal cord lesions. Front. Neurosci. 8, 59. https://doi.org/10.3389/fnins.2014.00059.

Cajal, R., 1928. Degeneration and Regeneration of the Central Nervous System. Oxford University Press, London, pp. 976.

Esposito, M.S., Capelli, P., Arber, S., 2014. Brainstem nucleus MdV mediates skilled forelimb motor tasks. Nature 5. https://doi.org/10.1038/nature13023.

Filli, L., Engmann, A.K., Zorner, B., Weinmann, O., Moraitis, T., Gullo, M., Kasper, H., Schneider, R., Schwab, M.E., 2014. Bridging the gap: a reticulo-propriospinal detour bypassing an incomplete spinal cord injury. J. Neurosci. 508 (7496), 351–356. https://doi.org/10.1523/JNEUROSCI.0701-14.2014.

Freund, P., Wannier, T., Schmidlin, E., Bloch, J., Mir, A., Schwab, M.E., Rouiller, E.M., 2007. Anti-Nogo-a antibody treatment enhances sprouting of corticospinal axons rostral to a unilateral cervical spinal cord lesion in adult macaque monkey. J. Comp. Neurol. 502 (4), 644–659. https://doi.org/10.1002/cne.21321.

Hasegawa, A., Takahashi, M., Satomi, K., Ohne, H., Takeuchi, T., Sato, S., Ichimura, S., 2016. Mechanism of forelimb motor function restoration after cervical spinal cord hemisection in rats: a comparison of juveniles and adults. Behav. Neurol. 2016. https://doi.org/10.1155/2016/1035473.

Imai, T., Aoki, M., 1993. Tracing of corticospinal fibers by extracellular pressure-injection of biocytin into the motor cortex in rats. Neurosci. Res. 16 (3), 229–233. https://doi.org/10.1016/0168-0102(93)90128-D.

Isa, T., 2006. Properties of propriospinal neurons in the C3–C4 segments mediating disynaptic pyramidal excitation to forelimb motoneurons in the Macaque Monkey. J. Neurophysiol. 95 (6), 3674–3685. https://doi.org/10.1152/jn.00103.2005.

Kinoshita, M., Matsui, R., Kato, S., Hasegawa, T., Kasahara, H., Isa, K., Watakabe, A., Yamamori, T., Nishimura, Y., Alstermark, B., Watanabe, D., Kobayashi, K., Isa, T., 2012. Genetic dissection of the circuit for hand dexterity in primates. Nature 487 (7406), 235–238. https://doi.org/10.1038/nature11206.

Martinez, M., Brezun, J.-M., Bonnier, L., Xerri, C., 2009. A new rating scale for open-field evaluation of behavioral recovery after cervical spinal cord injury in rats. J. Neurotrauma 26 (7), 1043–1053. https://doi.org/10.1089/neu.2008.0717.

Micheal, S., Erik, S., Udo, S., 2009. Kopt und Neuroanatomie PROMETHEUS Lern Atlas der Anatomie. First Japanese edition. Igaku-Shoin Ltd.

Nishimura, Y., Onoe, H., Onoe, K., Morichika, Y., Tsukada, H., Isa, T., 2011. Neural substrates for the motivational regulation of motor recovery after spinal-cord injury. PLoS One 6 (9), e24854. https://doi.org/10.1371/journal.pone.0024854.

Nunomaki, M., 2001. Morphological analysis of endogenous pain inhibitory system of the spinal trigeminal subnucleus caudalis in rats-neuronal tracing study using biotinylated dextran amine. J. Fukuoka Dent. Coll. 28 (4), 123–139.

Paxinos, G., Charles Watson, 2007. The Rat Brain in Stereotaxic Coordinates, 6th ed. Elsevier Academic Presshttps://doi.org/10.1016/0143-4179(83)90049-5.

Rasband, W.S., 2014. ImageJ. U.S. National Institutes of Health, Bethesda, Maryland, USA org/http://rsb.info.nih.gov/ij/. http://imagej.nih.gov/ij/.

Rosenzweig, E.S., Courtine, G., Jindrich, D.L., Brock, J.H., Ferguson, A.R., Strand, S.C., Nout, Y.S., Roy, R.R., Miller, D.M., Beattie, M.S., Havton, L.A., Bresnahan, J.C., Edgerton, V.R., Tuszynski, M.H., 2010. Extensive spontaneous plasticity of corticospinal projections after primate spinal cord injury. Nat. Neurosci. 13 (12), 1505–1510. https://doi.org/10.1038/nn.2691.

Sakakibara, S., Hoshikawa, K., Ishida, Y., Ngata, I., Omori, M., Terashi, H., Tahara, S., 2008. A nterpgrade labeling for hypoglossal nerve. J. Jpn. S R M 2128–2132.

Suemitsu, M., Utsunomiya, T., Yamamoto, K., 2012. ImageJ wo mochiita by-ourisosikigazou kaiseki-kouseihinosuuchika-(pathological organization image analysis using ImageJ - pumericalization of composition ratio-). Patholog. Clin. Med. 30 (4), 95–98.

Takahashi, M., Vattanajun, A., Umeda, T., Isa, K., Isa, T., 2009. Large-scale reorganization of corticofugal fibers after neonatal hemidecortication for functional restoration of forelimb movements. Eur. J. Neurosci. 30 (10), 1878–1887. https://doi.org/10.1111/j.1460-9568.2009.06989.x.

Takeuchi, T., Takahashi, M., Satomi, K., Ohne, H., Hasegawa, A., Sato, S., Ichimura, S., 2017. Mechanism of restoration of forelimb motor function after cervical spinal cord hemisection in rats: electrophysiological verification. Behav. Neurol. 2017. https://doi.org/10.1155/2017/7514681.

Tohyama, T., Kinoshita, M., Kobayashi, K., Isa, K., Watanabe, D., Kobayashi, K., Liu, M., Isa, T., 2017. Contribution of propriospinal neurons to recovery of hand dexterity after corticospinal tract lesions in monkeys. Proc. Natl. Acad. Sci. U. S. A. 114 (3), 604–609. https://doi.org/10.1073/pnas.1610787114.

Ueno, M., Hayano, Y., Nakagawa, H., Yamashita, T., 2012. Intraspinal rewiring of the corticospinal tract requires target-derived brain-derived neurotrophic factor and compensates lost function after brain injury. Brain (Pt 4), 1253–1267. https://doi.org/10.1093/brain/aws053.

Umeda, T., Isa, T., 2011. Differential contributions of rostral and caudal frontal forelimb areas to compensatory process after neonatal hemidecortication in rats. Eur. J. Neurosci. 34 (9), 1453–1460. https://doi.org/10.1111/j.1460-9568.2011.07866.x.

Umeda, T., Takahashi, M., Isa, K., Isa, T., 2010. Formation of descending pathways mediating cortical command to forelimb motoneurons in neonatally hemidecorticated rats. J. Neurophysiol. 104 (3), 1707–1716. https://doi.org/10.1152/jn.00968.2009.

Van Den Brand, R., Heutschi, J., Barraud, Q., DiGiovanna, J., Bartholdi, K., Huerlimann, M., Friedli, L., Vollenweider, I., Moraud, E.M., Duis, S., Dominici, N., Micera, S., Musienko, P., Courtine, G., 2012. Restoring voluntary control of locomotion after paralyzing spinal cord injury. Science 336 (6085), 1182–1185. https://doi.org/10.1126/science.1217416.

Weishaupt, N., Hurd, C., Wei, D.Z., Fouad, K., 2013. Reticulospinal plasticity after cervical spinal cord injury in the rat involves withdrawal of projections below the injury. Exp. Neurol. 247, 241–249. https://doi.org/10.1016/j.expneurol.2013.05.003.

Zörner, B., Bachmann, L.C., Filli, L., Kapitza, S., Gullo, M., Bolliger, M., Starkey, M.L., Röthlisberger, M., Gonzenbach, R.R., Schwab, M.E., 2014. Chasing central nervous system plasticity: the brainstem's contribution to locomotor recovery in rats with spinal cord injury. Brain 137 (Pt 6), 1716–1732. https://doi.org/10.1093/brain/awu078.